BATTERY CHARGE SYSTEM BASED ON BIDIRECTIONAL DC-DC CONVERTER EMPLOYING A DIGITAL CURRENT-MODE CONTROLLER FOR PHOTOVOLTAIC APPLICATIONS

Augusto de C. H. Damasceno, Henrique A. C. Braga and Pedro G. Barbosa

FEDERAL UNIVERSITY OF JUIZ DE FORA
Electrical Engineering Department
Campus UFJF, Juiz de Fora, MG
36036-330, Brazil

augusto@labsel.ufjf.br, henrique.braga@ufjf.edu.br and
pedro.gomes@ufjf.edu.br

***Abstract*— This work investigates the utilization of a predictive digital current-mode controller for a bidirectional DC-DC converter connected to a photovoltaic electric generation system. The DC-DC converter, with the digital current control, operates as a high performance battery charger system, enabling long battery life by providing precision charging control, constant monitoring and fast protection. Digital modeling of the converter and the controller are presented and discussed. Simulation results are used to validate the design controller procedures. The digital current-mode control was implemented in the DSP TMS320F2812 of Texas Instruments. Experimental results, obtained with a bidirectional DC-DC converter laboratory prototype, are presented to demonstrated the performance of the current-mode controller.**

***Index Terms*— Battery charger system, bidirectional DC-DC converter, digital current-mode control, predictive control, dead-beat control.**

I. INTRODUCTION

RENEWABLE energy sources based on photovoltaic (PV) cells have become an attractive technology to increase electrical energy supply. Their utilization have been motivated by factors such as: (*i*) reduction of the costs of the PV cells; (*ii*) lower transmission losses, since the generation system can be installed near the load; (*iii*) highly generation capability, due to the PV modularity; (*iv*) lower maintenance, due to the PV robustness and the absence of rotating parts and (*v*) the fact that the system is emission-free, [1] and [2].

However, the continuous supply of electrical energy in stand-alone or grid-connected PV systems is possible only by using energy sinks like battery banks. These batteries should store electrical energy from the PV cells during sunny periods, to supply it to the load during the night or overcast periods.

Figure 1 shows an example of three-phase grid-connected PV renewable energy source. In this figure the PV cells and the battery bank are connected to the system DC link through a DC-DC (boost) converter and a bidirectional DC-DC converter, respectively. This scheme permits the operation of the PV cells and the battery bank with different voltage levels.

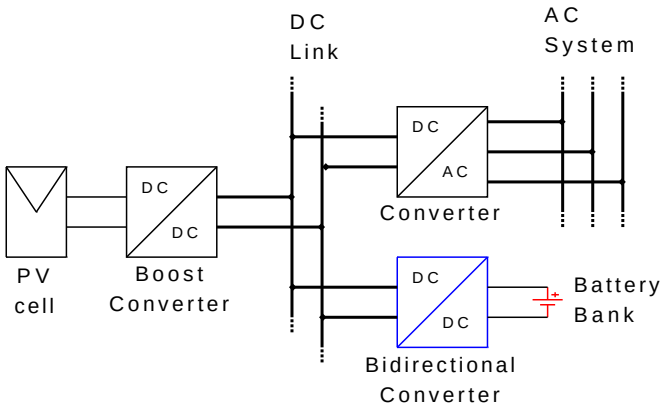

Fig. 1. Grid connected PV system with a battery bank connected in the DC-link through a bidirectional converter.

In these types of applications, lead-acid batteries are the most commonly used devices since it is possible to store large amounts of energy with a lower initial cost. However, many factors can reduce the lifetime of the batteries increasing their operational costs. One of the most important of them is the charge and discharge process which, in PV systems, is strongly influenced by the weather conditions and by the load demand, which will make the batteries used in PV systems have a different performance when compared to the batteries used in other applications, as example, uninterruptible power supplies (UPS).

In this way, an improved and secure mode of charging a battery can be obtained by using a four stages charge scheme. During the first two stages, the battery is charged with a constant current until its terminal voltage reaches a preestablished value. After that, during the

third and fourth stages, the charge controller is switched to a constant voltage operation to restore the battery full capacity. This scheme will provide a fast and secure charge of the battery by avoiding its overcharge [3].

The mode of discharge of a PV-system battery will depend on the load characteristic supplied by it. The three basic battery discharge schemes are: (a) constant resistance (the load current reduces as the battery voltage decreases since the resistance of the load remains constant); (b) constant current (the load current remains constant and independent of the battery voltage) and (c) constant power (the load current increases during the discharge while the battery voltage decreases). In these three discharge schemes, the discharge period will depend on the battery service time (hours of discharge).

As mentioned above, there are a variability of factors that influence the batteries capacity, performance and lifetime. However, the battery cycle control, or the mode of charge and discharge of the battery, can have a significant effect on the operational characteristic of it [4]. Hence, the improvement of the battery life will result a significant reduction of the operational system costs which, in some cases, can represent approximately 40 % of the total expenses [5].

Thus, the objective of this work is the study of a bidirectional DC-DC converter acting as battery charge/discharge controller. The bidirectional converter was designed with two control loops. The inner control loop is based on a predictive (dead-beat) current-mode control while the outer control loop controls the battery terminal voltage. The effectiveness of the proposed controller will be investigated through digital simulations and it was implemented in a TMS320F2812, Texas Instruments DSP, in such a way to control a 3 kW laboratory prototype.

II. The Bidirectional DC-DC Converter

Figure 2 shows the bidirectional DC-DC converter with its digital controller. The bidirectional converter is used in this work as interface converter between the PV-system DC link and the battery terminals. In this figure, v^*_{BB} and i^*_L are reference signals for the voltage and current control loops, respectively.

Since the voltages V_1 and V_2 are always positive, the real power at the converter terminals will be positive or negative, if and only if, the current can flow in both directions. In fact, this circuit can be viewed as a step-down (buck) converter, composed by S_1 and D_2, and a step-up (boost) converter, composed by S_2 and D_1 [6] and [7]. This converter capability permits the charge (buck stage) or the discharge (boost stage) of the battery bank, with controllable current or voltage, in similar way as those described in the previous section.

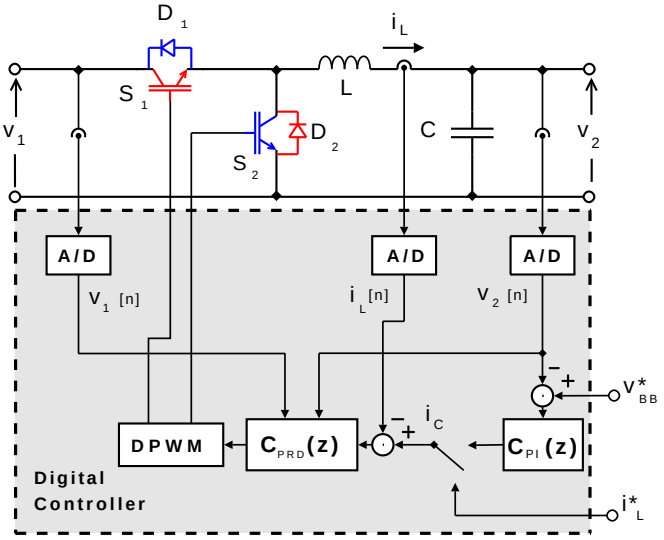

Fig. 2. Bidirectional DC-DC converter with its current and voltage control loops.

However, as the converter switches have bidirectional conduction current capability, it is possible to operate the bidirectional converter by changing the control signals of S_1 and S_2 in such a way to avoid the discontinuous conduction mode (DCM) of operation of the step-down and step-up stages. This functionality can be achieved by varying the duty ratio of the converter switches in an complementary way, that is, if d_1 is the control signal of S_1, the S_2 will be switched with a duty ratio $d_2 = (1 - d_1)$. Thus, not only the average amplitude of the output voltage and inductor current change, but the inductor current can also be positive and negative, leading to two-quadrant operation of the converter.

Thus, the bidirectional converter can drain energy from the battery to feed the load when the energy from the PV cells decreases as a consequence of the weather conditions. But it can also be controlled to charge the battery bank in a fast and secure manner during the periods when the PV cells convert more energy than that consumed by the load.

Another interesting aspect of the bidirectional DC-DC converter topology, shown in Fig. 2, is its easy implementation by using a half-bridge semiconductor module. This characteristic also simplify the effort to increase the capacity of the battery bank since many modules of bidirectional DC-DC converters can be connected in parallel in such a way to increase the current level between the DC link and the battery bank [8].

III. Principles of Predictive Digital Controller

Analog schemes based on current–mode control have been used successfully for controlling DC-DC as well single-phase power factor correction (PFC) converters. They are simple to implement, robust and reliable [9] and [10]. They can be classified as valley, peak or average current–mode controllers. Among these three schemes, the average current–mode control proposed by Dixon in [11] presents a better noise immunity in the current sense signal and it also has the advantage of operation with a constant frequency.

In spite of the success of the current-mode analog controllers, the modeling and the design of digital current-mode controllers have been receiving an increasing attention in the literature. The motivation of the digital implementations of these types of controllers can be explained by the reduction of the costs and the increase of processing capability of microcontrollers and digital signal processors (DSP).

In [12], the authors present and discuss the digital implementation of predictive, or dead-beat, current controller for DC-DC converters. The block diagram of this controller is shown inside the dashed rectangle in Fig. 2. In this figure, the block $C_{PRD}(z)$ has two additional inputs besides the error between the control current, i_C, and the inductor current, i_L.

In principle, the predictive control is a particular case of discrete time dynamic state feedback and direct pole allocation. The inductor current and the input and output converter voltages are sampled and used to determined the duty cycle of the next switching period in such a way to cancel the error between the reference current and the inductor current.

The reasoning behind the predictive current control is quite simple and can be explained referring to Fig. 3. In this figure, the reference current i_C is step changed before the instant $(n-1)T_S$. Then, considering $V_1 = V_{DC}$ and $V_2 = V_{BB}$ in the circuit of Fig. 2 and assuming that the inductor current is sampled every time the trailing triangular waveform reaches its zero value, it is possible to write the following difference equation for the bidirectional converter [12] and [13].

$$\begin{aligned} i_L[n+1] &= i_L[n] + \frac{V_{DC}-V_{BB}}{L} d[n] T_S - \\ &\quad - \frac{V_{BB}}{L} d'[n] T_S, \\ &= i_L[n] + \frac{V_{DC}}{L} d[n] T_S - \frac{V_{BB}}{L} T_S, \quad (1) \end{aligned}$$

where V_{BB} is the battery terminal voltage (V), V_{DC} is the DC link voltage (V), L is the converter inductance (H), $i_L[n]$ is the inductor current (A) sampled at the instant nT_S, $i_L[n+1]$ is the inductor current (A) that will be sampled at the instant $(n+1)T_S$, $f_S = (1/T_S)$ is the converter switching frequency (Hz), $d[n]$ is the converter duty ratio during the period nT_S and $d'[n] = 1 - d[n]$.

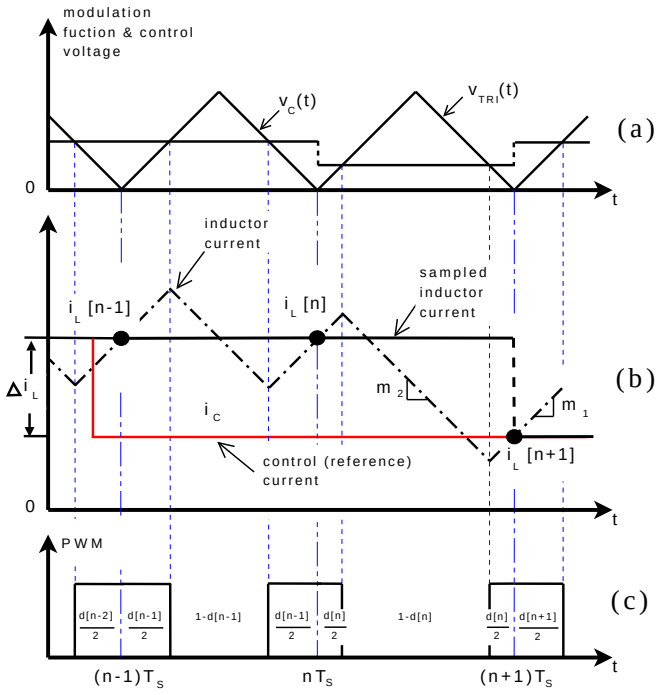

Fig. 3. Predictive current control waveforms: (a) Trailing triangle modulation and control voltage waveforms; (b) inductor current, sampled inductor current, and control (reference) current ($m_1 = (V_1 - V_2)/L$ and $m_2 = -V_2/L$); (c) PWM signal.

Using two consecutive sample periods to calculate the inductor current, the above equation can be rewritten as given bellow,

$$\begin{aligned} i_L[n+1] = i_L[n-1] - 2\frac{V_{BB}}{L} T_S + \\ + \frac{V_{DC}}{L} (d[n-1] + d[n]) T_S. \quad (2) \end{aligned}$$

Rearranging (2) and doing $i_L[n+1] = i_C$, the following control law can be written,

$$\begin{aligned} d[n] = -d[n-1] + \frac{L}{V_{DC} T_S} (i_C - i_L[n-1]) + \\ + 2\frac{V_{BB}}{V_{DC}}, \quad (3) \end{aligned}$$

where $d[n]$ is the duty ratio for the next sampled period and i_C is the control reference current (A). Note that the duty ratio $d[n]$ is calculated in the period $(n-1)T_S$ in such a way to force the inductor current i_L to be equal to the reference control current i_C at the end of period nT_S.

IV. Simulation Results

In this section, it will be shown some digital simulation results obtained with the alternative version of Electromagnetic Transients Program (ATP/EMTP). The DC-DC bidirectional converter of Fig. 2 was modeled in the EMTP. The predictive current mode and the digital voltage controllers were implemented using MODELS.

The MODELS is an EMTP general-purpose description language, supported by a set of simulation tools, for describing the dynamic behavior of complex physical systems. The MODELS environment was also used to model the sampling and the quantization effects of A/D circuits.

Table I shows the values of the main components used in the project of the bidirectional converter. The lead-acid battery was considering formed by 12 elements, with 2 V each, resulting in a 24 V nominal voltage.

TABLE I
BIDIRECTIONAL CONVERTER PARAMETERS.

Element		Value
Series inductor	(L)	175 μH
Output capacitor	(C)	235 μF
Switching frequency	(f_S)	25 kHz
DC Link Voltage	(V_{DC})	70 V

A. Inner Current Control Loop

The digital predictive current–mode controller was designed considering the mathematical equation given by (3). The sampling frequency of the inner current loop is 25 kHz. Fig. 4 (a) and (b) show the reference and the converter currents, and the battery terminal voltage, respectively. These results were obtained considering a simplified battery model, shown in Fig. 5, connected to the V_2 terminals of Fig. 2 circuit.

Initially the battery is charged with 50 A constant current. The battery voltage increases *linearly* until $t = 5$ ms. Then, the reference current is step changed from 50 A to -50 A. From this point until the end of the simulation time the battery supplies a constant current to the DC link. During this period the battery terminal voltage decreases *linearly*. These results show that the bidirectional converter, with its predictive current control, has the ability to operate in two quadrants of the *v-i* plane.

The drop, shown in Fig. 4 (b) between the charge and the discharge characteristics, is due to the internal voltage drop in the series resistance R_S of the battery model. The values of the capacitance C_{BB} and the resistance R_P were chosen in such a way to allow the observation of the charge and the discharge processes in a short simulation time. The chosen values of the C_{BB} and R_P are also responsible by the behavior almost linear of the voltage v_{BB} during the charge and the discharge processes.

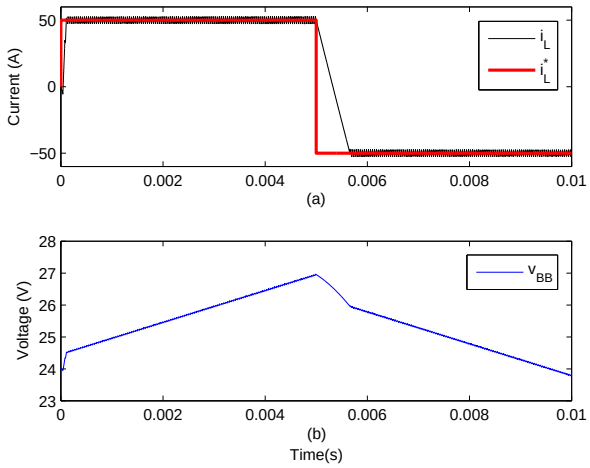

Fig. 4. (a) Reference current, i_L^*, and the inductor current, i_L; (b) output voltage, V_{BB}.

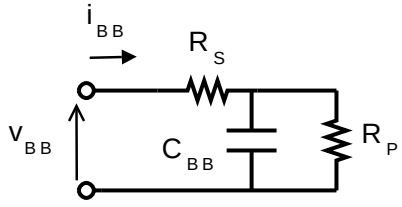

Fig. 5. Simplified model for the battery.

B. Outer Voltage Control Loop

An outer voltage control loop was designed in order to investigate the ability of the bidirectional converter to regulate the voltage at the terminals of the battery bank. Neglecting the effect of series resistance, R_S, the following transfer function can be written for the simplified battery model connected at the output terminals of the bidirectional converter with predictive current control.

$$G_v(s) = \frac{v_{BB}(s)}{i_L(s)} = \left(\frac{R_P}{\tau}\right)\left[\frac{1}{s+\frac{1}{\tau}}\right] \qquad (4)$$

where $\tau = R_P(C + C_{BB})$.

The discrete form of (4) can be obtained expanding its step response into partial fractions and using a $\mathscr{Z}$–transform table to find the discrete form of each one [14]. Then, multiplying each term by $\left(1 - z^{-1}\right)$, the following transfer function can be written in the z–domain as,

$$G_v(z) = \frac{v_{BB}(z)}{i_L(z)} = R_P \left[\frac{1 - e^{-(T/\tau)}}{z - e^{-(T/\tau)}} \right] \qquad (5)$$

In Fig. 3 it was shown that the predictive current control needs two switching periods, T_S, to track the control (reference) current, i_C. Thus, assuming that the sampling period T is higher than T_S, the instantaneous average value of $i_L(z)$ can be made equal $i_C(z)$ in (5), and the block diagram of Fig. 6 can be drawn for the voltage control loop of the bidirectional converter. The sampling period T must be chosen carefully since large values of T has detrimental effects on the relative stability of the system. In this application, good results were obtained doing T equals to eight to ten times higher than T_S.

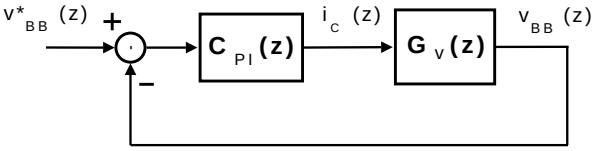

Fig. 6. Simplified discrete representation of bidirectional converter voltage control loop.

Based on Fig. 6, the gains of $C_{PI}(z)$ can be designed for a given maximum overshoot (M_p) and settling time (t_s). Thus, having in mind a standard second-order system response for $M_p = 0.2$, $t_s = 2\ ms$ and $T = 400\ \mu s$, the proportional an integral gains of the discrete PI are $0.100333\ A/V$ and $0.198552\ A/Vs$, respectively. These values were obtained doing $R_S = 0$, $R_P = 5\ \Omega$ and $C_{BB} = 0$ in the model of Fig. 5, which were chosen in order to reduce the time constant τ given in (4) consequently reducing the simulation time of the voltage control loop.

Figure 7 shows the root-locus of the system. The dominant closed-loop poles damping factor and the normalized damped natural frequency are $\xi = 0.45$ and $(\omega_d/\omega) = 0.088$, respectively, where $\omega_d = \omega_n\sqrt{1-\xi^2}$, $\omega = 2\pi/T$ and ω_n is the undamped natural frequency of dominant closed-loop poles.

Figure 8 (a) shows the control current, i_C, and the inductor current, i_L. As mention above, the sampling period of voltage control loop was chosen ten times higher than the predictive-current control loop period. Thus, while the output of the predictive controller is updated every $40\ \mu s$ $(25\ kHz)$, the output of the voltage controller is updated every $400\ \mu s$ $(2.5\ kHz)$.

Figure 8 (b) shows the converter output voltage, v_{BB}. The reference voltage has been set at $30\ V$. From $t = 0\ ms$ to $t = 10\ ms$ it is possible to see the step response of the compensated system. The percentage of measured overshoot is approximately 27 %, which is

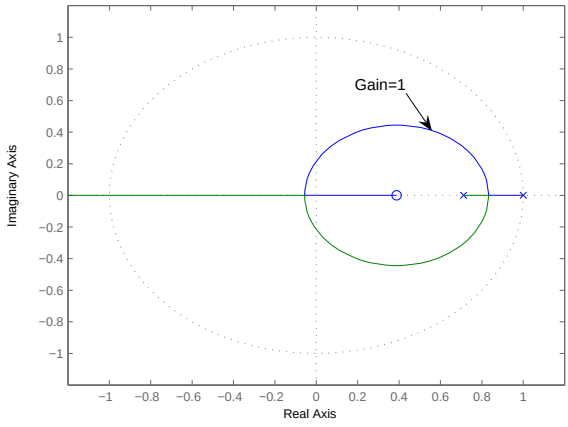

Fig. 7. Root Locus - outer loop.

more than the specified value of 20 %. This discrepancy can be explained by the fact that for large variations in control current i_C, like that observed in the beginning of the simulation time, the inductor current i_L delays more than $400\ \mu s$ to be equal to i_C. This behavior is also observed in Fig. 4 during the step variation of the control current.

In $t = 10\ ms$, R_P is switched from $5\ \Omega$ to $4\ \Omega$. After a small period during which the load voltage decreases the digital PI changes the control current, i_C, in such a way to regulate the output voltage to the reference value.

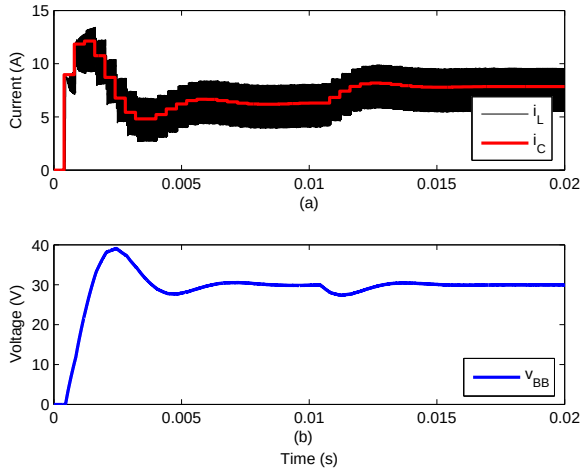

Fig. 8. (a) Reference, i_C, and inductor currents, i_L; (b) output voltage, v_{BB}.

C. AC Voltage Ripple Minimization

In [15], the authors present a general discussion about the discrepancies between the lifetime of the batteries predicted by manufacturers, normally obtained

in controlled laboratory conditions, and the time observed in the field applications, where the voltage and the temperature fluctuates. In practical applications, a poorly-regulated and unfiltered charge battery voltage and current will be responsible for premature failures and shortened battery life.

It is true that some AC ripple are inevitable in PV applications since the electrical energy converted by the PV cells is strongly dependent on the insolation conditions. In spite of the methods that can be used to minimize the charge ripple, this section has the objective to investigate the performance of the predictive current controller when some AC voltage ripple is present in the DC link converter voltage.

Figures 9 (a) and (b) show the inductor current and the output voltage when a 120 Hz sinusoidal voltage ripple with a 20 V of peak-to-peak amplitude is applied to the average the DC link voltage. Note that the predictive current controller with the outer voltage control loop regulates the output voltage of the bidirectional converter.

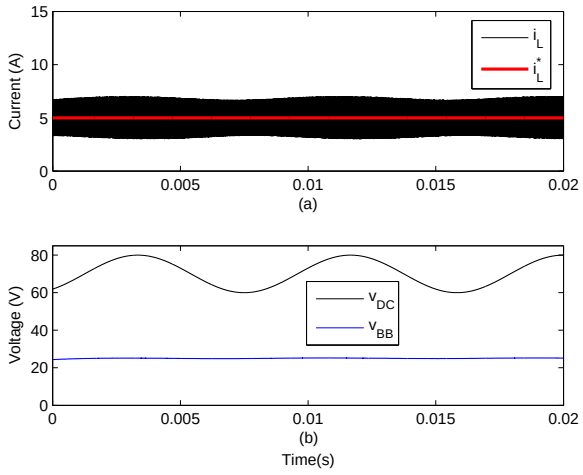

Fig. 9. AC Ripple voltage and current waveforms.

V. Experimental Results

A 3 kW DC-DC converter prototype was built to validated the simulation results and the controllers design procedures. The bidirectional converter uses two Semikron SK45GB63 IGBT modules connected in parallel. The digital predictive and voltage PI controllers were implemented using TMS320F2812 Texas Instruments DSP. The converter parameters are identical of those shown in Table I for the digital model.

Figure 10 shows the steady-state output voltage and current waveforms of the bidirectional converter. In this figure the battery was replaced by a resistance equals to $R = 8.4\ \Omega$. The converter switching frequency is $f_s = 25\ kHz$. The predictive controller assures that the inductor current tracks its reference value $(i_L^* = 5A)$.

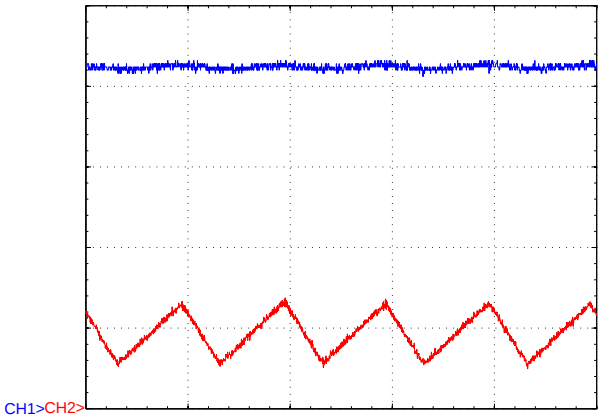

Fig. 10. Steady-state converter waveforms: output voltage (CH1⇒upper trace) and inductor current (CH2⇒lower trace). (*Horizontal scale*: 40 $\mu s/div.$; *Vertical scales*: CH1⇒ 10 $V/div.$ and CH2⇒ 5 $A/div.$)

Figure 11 shows the behavior of the converter output voltage and current when the load resistance is step changed from 8.4 Ω to 4.6 Ω. Note that since the load equivalent resistance is reduced the output voltage decreases due to the fact that the predictive controller holds the converter output current close to the reference value $(i_L^* = 5A)$.

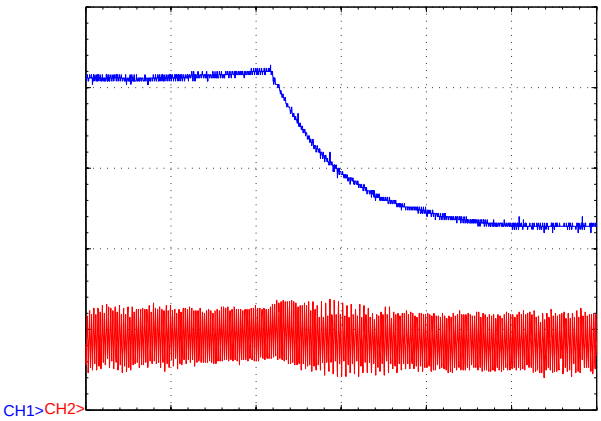

Fig. 11. Load variation: output voltage (CH1⇒upper trace) and inductor current (CH2⇒lower trace). (*Horizontal scale*: 1.3 $ms/div.$; *Vertical scales*: CH1⇒ 10 $V/div.$ and CH2⇒ 5 $A/div.$)

Figure 12 shows the converter output voltage and current when the reference current, i_L^*, is step changed continuously from 3 A to 5 A and vice-versa. This result was obtained using a square waveform signal, with frequency equals to 500 Hz, for the converter reference current and considering a load resistance, equals to 8.4Ω, connected to the output converter terminals. In this case the output voltage increases and decreases

linearly with the converter current as a consequence of the charge and the discharge of the output converter capacitor.

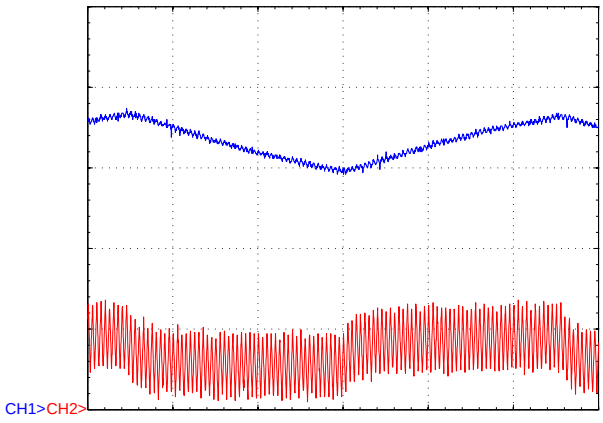

Fig. 12. Step variation from $3A$ to $5A$, and vice-versa, in the reference current signal (i_L^*): output voltage (CH1⇒upper trace) and inductor current (CH2⇒lower trace). (*Horizontal scale*: $0.8\ ms/div.$; *Vertical scales*: CH1⇒ $10\ V/div.$ and CH2⇒ $5\ A/div.$)

VI. Conclusions

This work describes the use of a predictive current–mode controller to control a bidirectional converter in such a way to provide a fast and secure charge and discharge of a battery bank connected to a PV generation system. The bidirectional converter used in this work is based on half-bridge semiconductor modules. This characteristic makes possible the operation of many modules in parallel in such a way to increase the capacity of the battery bank.

In spite of its simple processing requirement, the robustness and reliability of the predictive controller is strongly influenced by model mismatches and parameter uncertainties. The effect of model mismatches is normally unsafe once any deviation of the model given by (1) makes the controller action unpredictable. Alternatively, the parameter uncertainties cause system performance degradation and instabilities. Their effects can be compensated using tolerances for the converter parameters.

Another important parameter that must be chosen carefully is the PWM carrier waveform and the instant where the converter current is sampled (peak, valley or average). In this work it was used a trailing triangle waveform scheme and the inductor current has its average value sampled one time per switching period.

The predictive controller can be used to control other types of power electronics converters.

References

[1] R. L. Carletti, L. C. G. Lopes, and P. G. Barbosa, "A dispersed generation system based on photovoltaic cells: Converter configuration and switching strategies," in *Proceedings of COBEP'2003*. 7th Brazilian Power Electronics Conference, Sept. 2003, pp. 404–409.

[2] ——, "Active and reactive powers control scheme for a grid-connected photovoltaic generation system based on vsi with selective harmonic elimination," in *Proceedings of COBEP'2005*. 8th Brazilian Power Electronics Conference, June 2005, pp. 129–134.

[3] L. Balogh, "Implementing multi-state charge algorithm with the UC3909 switchmode lead-acid battery charger controller," *Unitrode Application Note, U-155*, pp. 1–29, 1995.

[4] R. H. Rosemback, "Conversor cc-cc bidirecional buck-boost atuando como controlador de carga de baterias em um sistema fotovoltaico," Master dissertation, Universidade Federal de Juiz de Fora, Programa de Pós-Graduação em Engenharia Elétrica, Nov. 2004.

[5] S. Duryea, S. Islam, and W. Lawrance, "A battery management system for stand-alone photovoltaic energy systems," *IEEE Industry Applications Magazine*, vol. 7, pp. 67–72, May/June 2001.

[6] L. Schuch, C. Rech, H. L. Hey, H. A. Gründling, H. Pinheiro, and J. R. Pinheiro, "Análise e projeto de um conversor bidirecional PWM de alto desempenho para interface entre o barramento CC e o banco de baterias," *Revista Brasileira de Eletrônica de Potência (SOBRAEP)*, vol. 9, no. 1, pp. 1–11, June 2004.

[7] A. Emadi, A. Nasiri, and S. B. Bekiarov, *Uninterruptible Power Supplies and Active Filters*. CRC Press, 2005.

[8] F. A. Himmelstoss, "Analysis and comparison of half-bridge bidirectional DC-DC converters," in *25th Annual IEEE Power Electronics Specialists Conference, PESC'94 Record*, vol. 2, June 1994, pp. 922–928.

[9] U. Supatti, S. Boonto, C. Prapanavarat, and V. Moneyakul, "Design of an H_∞ robust controller for multi-module parallel dc-dc buck converters with average current mode control," in *Industrial Technology, 2002. IEEE ICIT'02*. IEEE, Dec. 2002, pp. 992 – 997.

[10] J. Sun and R. M. Bass, "Modeling and practical design issues for average current control," in *Fourteenth Annual Applied Power Electronics Conference and Exposition*, vol. 2, March 1999, pp. 980 – 986.

[11] L. Dixon, "Average current mode control of switching power supplies," *Unitrode Application Note, U-140*, pp. 356–369, 1990.

[12] J. Chen, A. Prodić, R. W. Erickson, and D. Maksimović, "Predictive digital current programmed control," *IEEE Transactions on Power Electronics*, vol. 18, no. 1, pp. 411–419, Nov. 2003.

[13] P. Andreassen and T. M. Undeland, "Digital control techniques for current mode control of interleaved quasi square wave converter," in *Power Electronics Specialists Conference. PESC'05*, IEEE. 36th, 2005, pp. 910–914.

[14] K. Ogata, *Discrete-Time Control Systems*, 2^{nd} ed. Prentice Hall, 1994.

[15] R. F. Nelson and M. A. Kepros, "AC ripple effects on VRLA batteries in float applications," in *The Fourteenth Annual Battery Conference on Applications and Advances*, Jan. 1999, pp. 281–289.